International Journal of Nanomedicine

Dovepress
open access to scientific and medical research

Open Access Full Text Article

ORIGINAL RESEARCH

Inhibition of cancer cell migration with CuS@mSiO$_2$-PEG nanoparticles by repressing MMP-2/MMP-9 expression

This article was published in the following Dove Press journal:
International Journal of Nanomedicine

Guoying Deng,[1,*] Feng Zhou,[1,*] Zizheng Wu,[2–4] Fei Zhang,[1] Kerun Niu,[2,3] Yingjie Kang,[5] Xijian Liu,[6] Qiugen Wang,[1] Yin Wang,[7] Qian Wang[1]

[1]Trauma Center, [2]Department of Orthopaedics, Shanghai General Hospital, Shanghai Jiaotong University School of Medicine, [3]Department of Orthopaedics, Shanghai General Hospital of Nanjing Medical University, [4]Department of Orthopaedics, Baoshan Branch of Shanghai General Hospital of Shanghai Jiaotong University, [5]Department of Radiology, Shuguang Hospital, Shanghai University of Traditional Chinese Medicine, [6]College of Chemistry and Chemical Engineering, Shanghai University of Engineering Science, [7]Ultrasound Department of Shanghai Pulmonary Hospital, Tongji University, Shanghai, People's Republic of China

*These authors contributed equally to this work

Correspondence: Qian Wang
Trauma Center, Shanghai General Hospital, Shanghai Jiaotong University School of Medicine, 650 Xin Songjiang Road, Shanghai 201620, People's Republic of China
Tel +86 136 6169 8212
Email drwangqian23@126.com

Yin Wang
Ultrasound Department of Shanghai Pulmonary Hospital, Tongji University, Shanghai 200433, People's Republic of China
Tel +86 137 0188 5138
Email lpbbl@aliyun.com

Abstract: The metastasis of cancer cells is a vital aspect of disease progression and therapy. Although a few nanoparticles (NPs) aimed at controlling metastasis in cancer therapy have been reported, the NPs are normally combined with drugs, yet the direct therapeutic effects of the NPs are not reported. To study the direct influence of NPs on cancer metastasis, the potential suppression capacity of CuS@mSiO$_2$-PEG NPs to tumor cell migration, a kind of typical photothermal NPs, was systemically evaluated in this study. Using CuS@mSiO$_2$-PEG NP stimulation and a transwell migration assay, we found that the migration of HeLa cells was significantly decreased. This phenomenon may be associated with two classical proteins in metastasis: matrix metalloproteinase 2 (MMP-2) and matrix metalloproteinase 9 (MMP-9). In addition, the mechanism may closely associate with non-receptor tyrosine kinase protein (SRC)/focal adhesion kinase (FAK) signaling pathway which varies in vivo and in vitro. To confirm the differences in the expression of SRC and FAK, related inhibitors were studied for additional comparison. Also, the results indicated that even though the migration inhibition was closely related to SRC and FAK signaling pathway, there may be another unknown regulation mechanism existing and its metastasis inhibition was significant. Confirmed by long-term survival curve study, CuS@mSiO$_2$-PEG NPs significantly reduced the metastasis of cancer cells and improved the survival rates of metastasis in a mouse model. Thus, we believe that the direct influence of NPs on cancer cell metastasis is a promising study topic.

Keywords: metastasis inhibition, photothermal nanoparticles, SRC/FAK signaling pathway, survival curves, MMPs

Introduction

In recent decades, many efforts have been made to develop nanoparticles (NPs) for cancer therapy. Various types of NPs have proven effective in numerous applications in medical diagnostics and treatment.[1] Briefly, the functions of nanomedicine include site-directed drug delivery,[2] imaging or tracing,[3] and even immunomodulation.[4] Moreover, the potential of multifunctional theranostic systems is similar to that of photothermal therapy (PTT)[5] or optical imaging applications[6] in addition to that of the direct influence of the NPs.[7]

Besides, interference techniques, such as PTT and drug delivery systems, have been widely used. New methods, such as magnetic hyperthermia,[8] radio sensitizers,[9] targeted drug delivery systems,[10] absorbance in the near-infrared (NIR) region,[11] and multifunctional core–shell structures,[12] in addition to other attempts, have been used as upgrades, with the goal of accurately and effectively destroying cancer cells.

submit your manuscript | www.dovepress.com
Dovepress
http://dx.doi.org/10.2147/IJN.S148487

However, destroying cancer cells topically never fulfills the aim of cancer therapy.[13] The unlimited proliferation and metastasis, rather than the tumor at the primary site, lead to the high mortality of cancers. Precision medicine is often in conflict with extended radical resection. Clinically, if any of the tumor survives and metastasis occurs, the entire therapy has technically failed,[14] leading to high death rates.[15] Meanwhile, topical interference, such as PTT, can lead to severe local damage, and the structural collapse of blood vessels may promote potential metastasis.[16] Therefore, inhibiting metastasis may be more essential for local tumor destruction. Moreover, subsequent changes in the microenvironment play a vital role in the generation and development of a tumor,[17] which cannot be ignored in a thorough cancer therapy. Thus, more attention should be paid to the other effects of NPs in biomaterial cancer studies.

Although metastasis-suppressing functions have been considered in recent years, researchers have focused on loading constituents, such as drug modifications[18] or siRNA integration.[19] The metastasis-suppressing potential of NPs themselves, rather than the loading drugs, remains a novel study area. Relevant signaling pathways and receptors are new targets for multifunctional NPs. In this case, to ensure that the possible new function occurs, models that have better explanatory power should be developed prior to models that describe the clinical disease progression. The typical indices and classical methods should be used for new discoveries.

Cell migration is particularly relevant to cancer progression. The migratory activity of tumor cells is a critical step within the metastatic cascade that leads to the settling of tumor cells in distant organs.[20–22] As a typical and classical index of cancer metastasis, cell migration and two classical signaling pathway receptors, focal adhesion kinase (FAK) and non-receptor tyrosine kinase protein (SRC), were investigated in this study.

The CuS NPs used in this study are a typical example of the particles used in PTT, which has been shown to be a promising alternative or supplement to traditional cancer therapies.[23,24] CuS@mSiO$_2$-PEG NPs were studied in our previous experiments.[25] As an NIR light-responsive drug delivery system, these NPs were again used for a metastasis investigation in this study. This time, only the direct influence (without PTT or controlled drug release) was investigated. For this reason, the PTT function and its therapy effects were not involved in this study.

To evaluate the possibility and potential of NPs in tumor metastasis inhibition, a detailed study on the effects of CuS@mSiO$_2$-PEG NPs on the migration of cancer cell lines, both in vitro and in vivo will be presented. After evaluation of the basic characteristics and biosafety, migration suppression phenomena were identified by transwell systems and RT-PCR. Then, the proteins of relevant signaling pathways were systematically detected in vitro and in vivo and included matrix metalloproteinase 2 (MMP-2), matrix metalloproteinase 9 (MMP-9), SRC, and FAK. Moreover, inhibitors were studied for additional confirmation. Finally, the metastasis-suppressing function was evaluated in a nude mouse tumor metastasis model.

Materials and methods

Synthesis of CuS@mSiO$_2$-PEG core–shell NPs

CuS@mSiO$_2$-PEG core–shell NPs were prepared according to our previous method[25] and were characterized by transmission electron microscopy (TEM; JEM-2100F) and X-ray diffraction using a D/max-2550 PC X-ray diffractometer (XRD; Cu-Kα radiation; Rigaku, Tokyo, Japan). The NPs were also characterized via the temperature elevation of pure water (a control experiment) and aqueous dispersions containing CuS@mSiO$_2$-PEG NPs at different concentrations under irradiation with a 980-nm laser at a power density of 0.51 W/cm^2. As-synthesized CuS@mSiO$_2$-PEG NPs were dispersed in deionized water for further use.

After characterization, the NPs were dispersed in an aqueous solution at a concentration of 5 mg/mL and sterilized by 25 kGy cobalt 60 (the test–retest method showed that the synthesis was not changed by this radiation level).

Culture of the cancer cell lines

The HeLa cell line is one of the most commonly used cell lines in all types of investigations,[26] especially in biomaterial cancer therapy investigations.[27] Because no typical cell type has been reported for this study of direct metastasis inhibition, the HeLa cell line was suitable because of its universality and specificity.

HeLa cell line obtained from the American Type Culture Collection (ATCC, Manassas, VA, USA) was cultured in DMEM/F12 (Thermo Fisher Scientific, Waltham, MA, USA), supplemented with 10% fetal bovine serum (FBS; Thermo Fisher Scientific) and 1% penicillin/streptomycin in T175 (Corning Incorporated, Corning, NY, USA) at a concentration of 2×10^5/mL. The cells were incubated in a humidified atmosphere of 5% CO_2 at 37°C to cultivate cells in vitro.

Biosafety and direct flow cytometry analysis

The metastasis in vivo and migration in vitro of tumor cell lines is closely related to the level of proliferation.[28]

Biosafety was evaluated based on the absorbance of the NPs. Prior to Cell Counting Kit-8 (CCK-8) analysis, the evaluation of possible influence of CuS@mSiO$_2$-PEG NPs on CCK-8 and the cytometry analyses were performed separately. First, NPs were directly added to 96-well plates at different gradient concentrations (0, 25, 50, 100, 200, and 400 μg/mL) in culture medium, and the absorbance at 490 nm was measured by a micro-plate reader. Then, digested HeLa cells were directly cultured with NPs at a concentration of 80 μg/mL for 15 min and tested on an Accuri C6 using the fluorescence channels for fluorescein isothiocyanate (FITC), phycoerythrin/propidium iodide (PI), 7-amino actinomycin D, and allophycocyanin (APC) afterward. After the credibility of these results was ensured, the biosafety of the CuS@mSiO$_2$-PEG NPs was tested.

To determine the toxicity of the NPs, HeLa cells were seeded into 96-well plates (1×10^4 cells/well). After 24 h, the top layer of the medium was exchanged with medium containing different concentrations of NPs (0, 20, 40, 80, and 100 μg/mL) that were dispersed by ultrasound. After another 24 h, a 10% CCK-8 (Dojindo Laboratories, Kumamoto, Japan) solution was added to each well, according to the manufacturer's instructions. Data were collected from three separate experiments with four replications each time. Before the comparison, the absorbance was normalized to that of a control group without NPs.

For apoptosis analysis, HeLa cells were pre-stimulated for 24 h by 80 μg/mL NPs. The control group was digested and then incubated with 5 μL of APC–Annexin V and 5 μL of PI for 15 min at room temperature (25°C) in the dark. Next, 400 μL of 1× binding buffer was added to each tube and then analyzed on an Accuri C6 (BD, Franklin Lakes, NJ, USA).

Biocompatibility and stability tests in vivo

Animal preparation

This study was performed following the National Institutes of Health guidelines for the use of experimental animals, and all animal protocols were approved by the Institutional Animal Care and Use Committee of Shanghai Jiaotong University. Eight male BALB/c nude mice were subcutaneously injected with 5×10^6 HeLa cells on both sides of the back. The cells injected in the left side were pre-stimulated with 80 μg/mL NPs for 24 h before digestion. The tumor volume was measured on days 3, 5, 7, 9, and 12 after the cell injections. The tumor volume was calculated according to the formula: volume $=0.5\times$ length $\times$ width^2. Two weeks after the subcutaneous injections, the samples were isolated for Cu elemental determination by inductively coupled plasma atomic emission spectrometry (ICP-AES). In the case of an uneven distribution of NPs, several parts from one tumor were separately used for detection, and the remaining portion of the tumor was used for Western blot analysis, as follows.

Migration detection and RT-PCR detection of functional proteins MMP-2/MMP-9

In the cell migration assay, 4×10^4 cells were suspended in 200 μL of serum-free DMEM–F12 medium with or without 80 μg/mL NPs; the cells were then seeded into the upper chamber of separate inserts. Next, 500 μL of DMEM–F12 containing 10% FBS was added to the 24-well plates. After incubation at 37°C for 12–14 h, the cells that migrated were fixed and stained for 30 min in a 0.1% crystal violet solution in PBS. After sufficient washing in PBS, the cells in the upper inserts were carefully removed using swabs. The cells were imaged using a Leica DFC350 FX microscope and Leica Application Suite LAS AF AF6000 software (Leica Microsystems, Wetzlar, Germany).

In addition, RNA was isolated from HeLa cells (experimental group: 24 h stimulation by 80 μg/mL NPs in culture medium) with TRIzol reagent (Thermo Fisher Scientific, Waltham, MA, USA) according to the manufacturer's instructions (Thermo Fisher Scientific). Complementary DNA (cDNA) was synthesized with a PrimeScript RT Reagent Kit (Takara, Kusatsu, Japan). Given the close correlation between migration and MMPs,[29] the MMP-2 (forward primer: gtcgcccatcatcaagttcc; reverse primer: gcatggtctcgatggtgttc) and MMP-9 (forward primer: ccaccgagctatccactcat; reverse primer: ggtccggtttcagcatgttt) expression levels were detected. The reference gene GAPDH (forward primer: ggcaagttcaacggcacagt; reverse primer: atgacatactcagccggc) was used as an internal control. Then, the cDNAs were amplified by quantitative RT-PCR (qRT-PCR) using AceQ SYBR Master Mix (Vazyme, Nanjing, China) on a 7900HT system, and the fold changes were calculated by relative quantification ($2^{-\Delta\Delta Ct}$).

Western blot analysis of SRC-related signaling pathway proteins

HeLa cells were stimulated by CuS@mSiO$_2$-PEG NPs at different concentrations (0, 20, 40, or 80 μg/mL) for 48 h; subsequently, cell lysates and ground tissues from in vivo samples were prepared in mammalian protein extraction buffer (Biotech Well, Shanghai, China). The supernatants obtained after centrifugation at 12,000× *g* for 15 min at 4°C were used for Western blot analyses. The protein concentration was measured by colorimetric analysis (Bio-Rad Laboratories Inc., Hercules, CA, USA) according to the method of Cheng et al.[30] Proteins were fractionated by sodium dodecyl sulfate polyacrylamide gel electrophoresis (SDS-PAGE) and transferred to a polyvinylidene fluoride (PVDF) transfer membrane (EMD Millipore, Billerica, MA, USA), and nonspecific binding sites were blocked with SuperBlock-tris-buffered saline (Biotech Well). The membranes were then incubated with primary antibodies for 12 h at 4°C with gentle agitation. Next, the immunoreactivity was detected with horseradish peroxidase-conjugated IgG (Biotech Well), an electrochemiluminescence kit (Biotech Well), and film autoradiography. The immunoreactivity was quantified with a Kodak Digital Science Image Station. The following primary antibodies were used: SRC (Cell Signaling Technology, Danvers, MA, USA), FAK (Cell Signaling Technology), MMP-2 (Abcam, Cambridge, MA, USA), and MMP-9 (Abcam). The housekeeping gene GAPDH (Cell Signaling Technology) was used as an internal control. All experiments were repeated three times.

Further confirmation of signaling pathways by inhibitors

Metastasis suppression was shown, and the potential regulatory protein levels changed significantly. To clarify the relationship between the SRC/FAK signaling pathway and the MMP-2/MMP-9 suppression related to the treatment by the CuS@SiO$_2$ NPs (80 μg/mL), the SRC inhibitor PP1 (Santa Cruz Biotechnology Inc., Dallas, TX, USA) and FAK inhibitor 14 (Santa Cruz Biotechnology Inc.) were used separately in migration experiments (1 μmol/mL) to clarify the variations in SRC and FAK.

Suppression function evaluation in a nude mouse tumor metastasis model

To clarify and definitively evaluate the inhibition function, a special metastasis model was needed rather than a disease model. The mechanism underlying the metastasis after PTT is based on two preconditions: first is the presence of residual cancer cells after PTT, which is quite possible in practice. Second is the structural indiscriminate damage to the circulation system, which can strongly promote the process of metastasis.[31] To imitate the situation quantitatively, a lung metastasis model was established by intravenous injections based on previous report.[32] Briefly, a single cell suspension of HeLa cells was prepared for tail vein injection. Mice were intravenously injected in the tail vein using insulin syringes with 1×10^6 tumor cells in 100 μL of PBS. Before injection, based on the uptake and degradation of NPs absorbed,[33,34] the cells in the experimental group were pre-stimulated with 80 μg/mL NPs for 24 h to ensure sufficient absorption. After injection, the nude mice were observed daily, and survival curves were constructed. At the end of the timeline (40 weeks), lung samples were removed, infused with Bouin's fixative, and then processed for hematoxylin–eosin staining. Considering the possible higher demise in the control group, mice in that group were sacrificed when serious dyscrasia was observed (1–2 days before death, for the last five samples based on previous data). Images were acquired using a Leica DFC350 FX microscope and Leica Application Suite LAS AF AF6000 software.

Statistical analysis

All results are presented as mean ± standard deviation. Data were collected in GraphPad Prism 5 (GraphPad Software, Inc., La Jolla, CA, USA) and analyzed using SPSS 21.0 software (IBM Corporation, Armonk, NY, USA). Statistical analyses were conducted using one-way analysis of variance (ANOVA). For survival analysis, Kaplan–Meier survival curves were constructed, and the differences between them were tested by the log-rank test. A P-value of <0.05 was considered statistically significant.

Results

The NPs used in the following experiments were identified as CuS@SiO$_2$ NPs as reported previously. Their core–shell structure was characterized by TEM (Figure 1A and B), and the phase structure of the resulting NPs was examined by the XRD pattern (Figure 1C). The optical properties of aqueous dispersions of CuS@SiO$_2$ NPs at different concentrations were also determined (Figure 1D). The temperature elevation of pure water increased with increasing NP concentration (Figure 1E). As the concentration increased, the temperature change (ΔT) increased significantly (Figure 1F). Based on the information of our previous study,[25] the NPs used in the following experiments were CuS@SiO$_2$ NPs. In addition, the CuS@SiO$_2$ NPs demonstrated low absorbance and fluorescence (Figures S1–S3), indicating a low interference in

CCK-8 tests or flow analyses. In these tests, the cell viability exhibited no significant difference from the control until the interference concentration reached 160 μg/mL (Figure 1G and H). No significant apoptosis was detected after pre-stimulation with CuS@SiO$_2$ NPs (Figure S4); thus, the CuS@SiO$_2$ NPs are biocompatible in vitro. For further biosafety injected in vein (1 mg/kg, 48 h) was evaluated by the blood biochemistry test, compared with the control group no significant differences were found either.

Normally, tumor growth and metastasis are closely and positively related.[35] In order to clarify the possible influence that Cus@SiO$_2$ NPs have, HeLa cells per-treated with/without NPs were used for dorsal subcutaneous tumor implant tests on different sides in same nude mice. Two weeks after the subcutaneous injection of HeLa cells, tumors of the recipient mice were harvested to survey the tumor volume and Cu content. Interestingly, tumors from the experimental group appeared green, indicating the presence of Cu (Figure 2A),

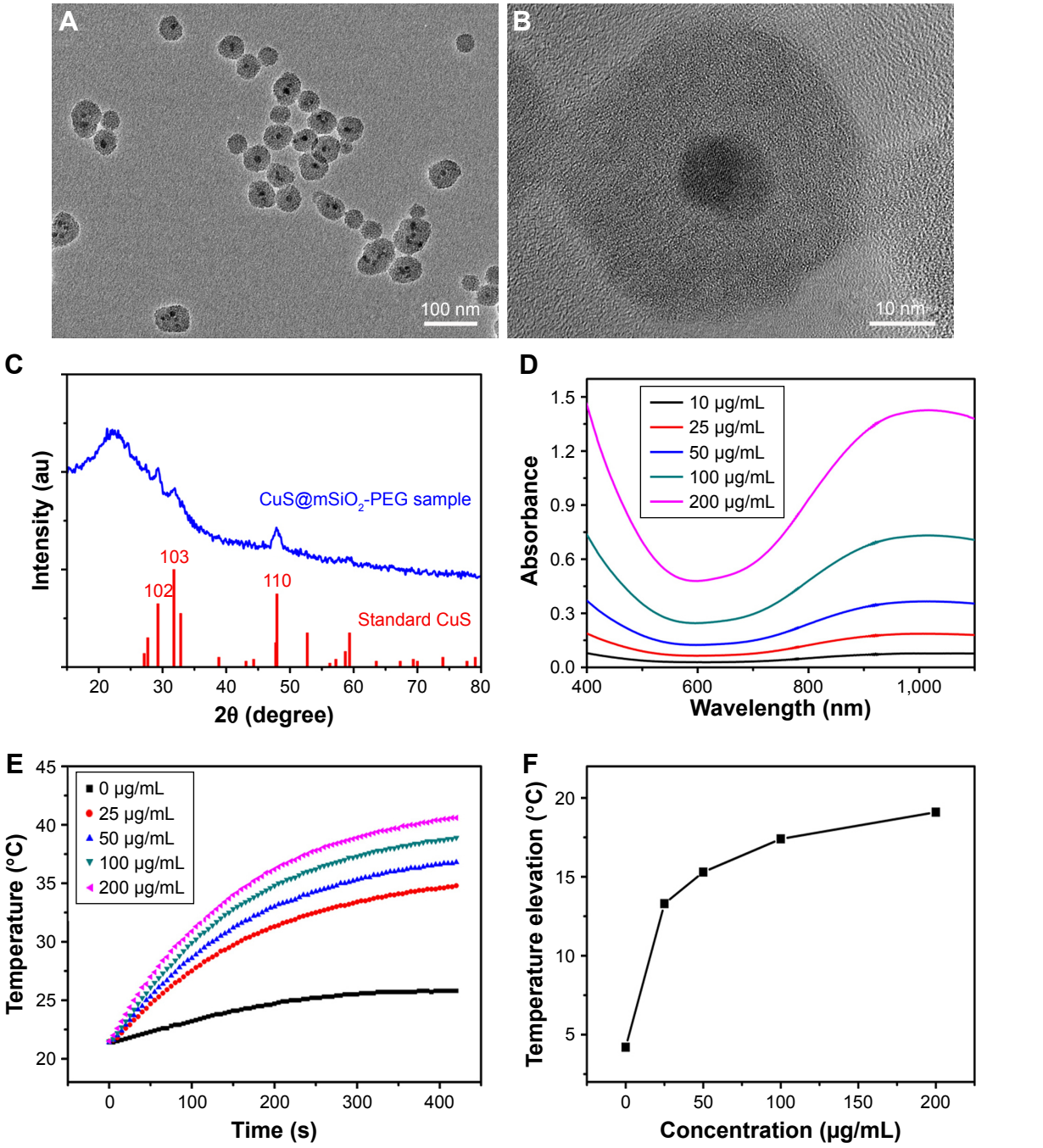

Figure 1 (*Continued*)

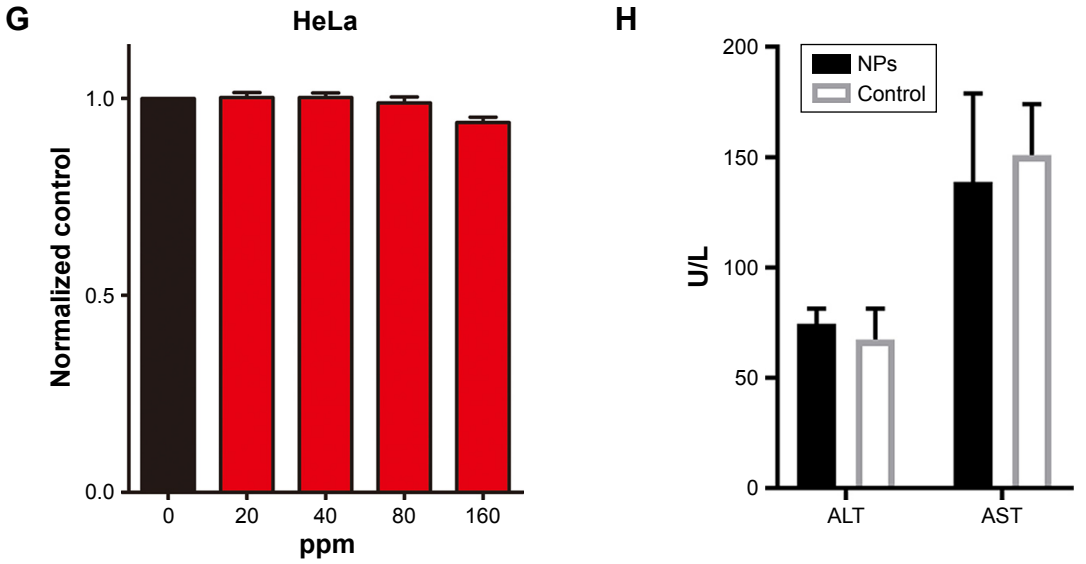

Figure 1 Low (**A**) and high magnification (**B**) TEM image of the CuS@SiO_2 NPs. XRD pattern (**C**) of the CuS@SiO_2 NPs and the standard hexagonal phase of Cu (JCPDS card no: 06-0464). Absorption spectrum (**D**) for various concentrations of hydrophilic CuS@SiO_2 NPs. Temperature elevation of pure water and of an aqueous dispersion of CuS@SiO_2 NPs at different concentrations (0, 25, 50, 100, or 200 μg/mL) as a function of irradiation time (5 min). Pure water was used as a control, and the room temperature was 25°C (**E**). The temperature change (ΔT) over a period of 5 min has a significant positive correlation with the CuS@SiO_2 NP concentration of the aqueous dispersion (**F**). The toxicity of the CuS@SiO_2 NPs was evaluated by CCK-8 tests as a function of incubation concentration (0–160 ppm) for the HeLa cells (**G**). ALT and AST in blood biochemistry test (**H**). Cells were incubated with the solutions at 37°C for 24 h.

Abbreviations: CCK-8, Cell Counting Kit-8; NP, nanoparticle; TEM, transmission electron microscopy; XRD, X-ray diffractometer.

which was also detected by ICP-AES. Compared with the value in the control group (0.312±0.026 μg/g), the Cu content increased significantly (85.5±11.828 μg/g; Figure 2C). Therefore, the pre-stimulated CuS@SiO_2 NPs were absorbed by the HeLa cells. However, the tumor volume did not show

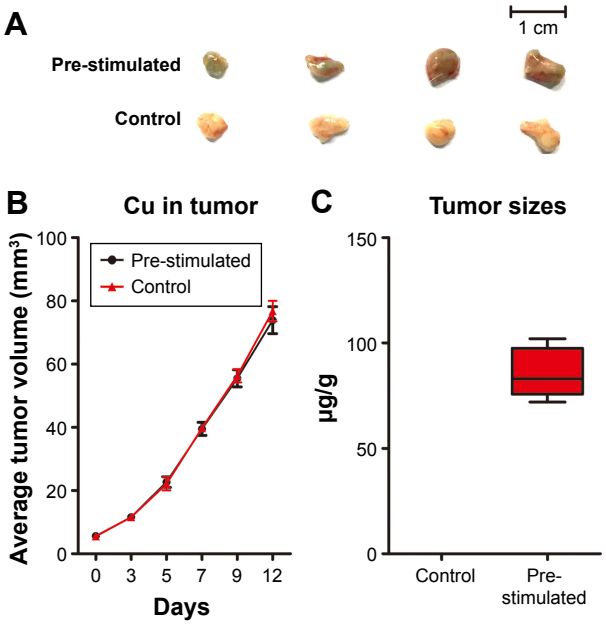

Figure 2 Two weeks after subcutaneous injection of HeLa cells, tumors from the experimental group appeared green (**A**). The tumor size increased with time. However, the sizes of the two groups showed no significant difference ($P>0.05$). The stability and biosafety were fully verified in vivo (**B**). The Cu content was significantly higher in the tumors than in the control group (**C**) ($P<0.05$).

any significant differences in any of the groups (Figure 2B), indicating minor growth interference of the CuS@SiO_2 NPs in vivo and suggesting that the migration decrease due to pre-stimulation was not a result of growth inhibition.

CuS@SiO_2 NPs showed suppression effects on the HeLa cell migration in vitro. A transwell-based migration assay was performed to quantitatively evaluate the migration after stimulation with CuS@SiO_2 NPs. As shown in Figure 3, compared with the value in the control group, the average number of migrated HeLa cells decreased significantly with treatment by 80 μg/mL CuS@SiO_2 NPs ($P<0.05$; Figure S5). Furthermore, RT-PCR indicated decreased expression of MMP-2/MMP-9 in HeLa cells as a function of concentration. The MMP-2/MMP-9 expression of stimulated cells decreased significantly following treatment with 20, 40, or 80 μg/mL CuS@SiO_2 NPs compared with that in the control group (Figure 3). The tendency did not precisely vary with concentration. These results confirmed the data obtained from the transwell-based migration assay. The migration-inhibiting capacity of CuS@SiO_2 NPs and a possible connection with MMP-2/MMP-9 were detected. Stimulation with CuS@SiO_2 NPs for 24 h caused downregulation of MMP-2 and MMP-9 ($P<0.05$). The related signaling pathway is considered in the following mechanism study.

The CuS@SiO_2 NPs mediated the expression of migration-related proteins. After stimulation for 48 h (80 μg/mL), the expression of MMP-2, MMP-9, SRC, and FAK decreased

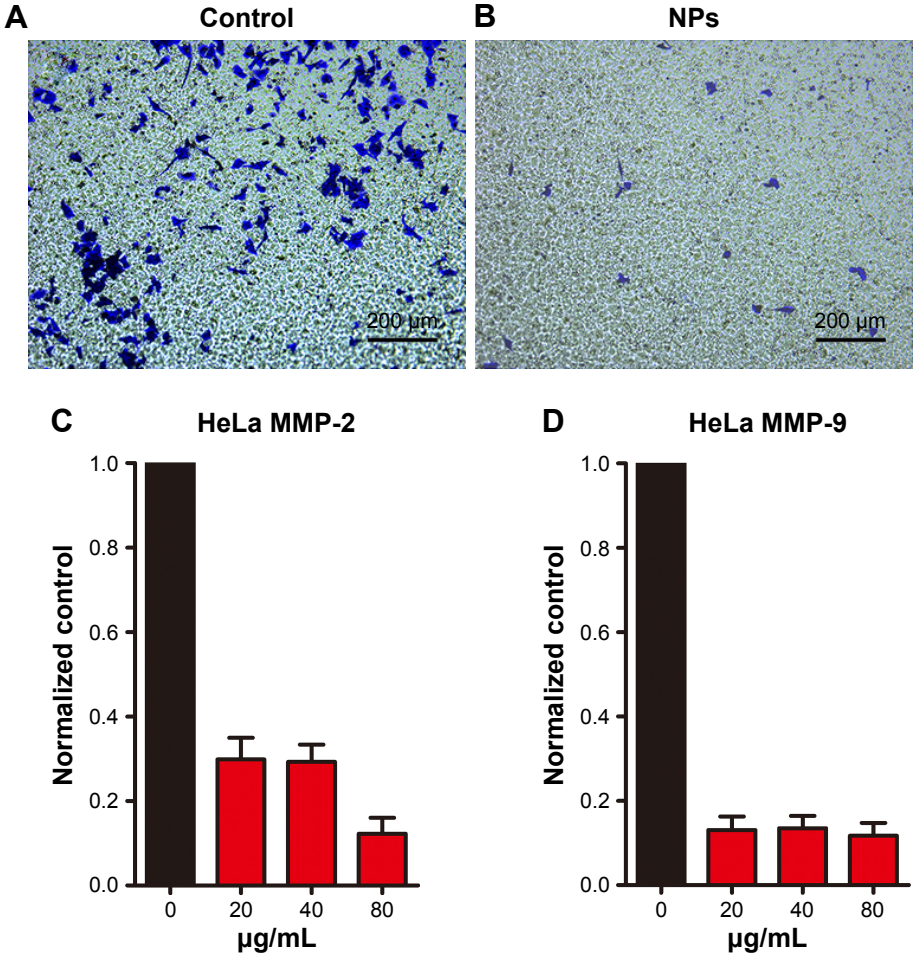

Figure 3 HeLa cell migration was observed for 14 h using a transwell migration assay (**A**). The HeLa cell migration induced by 80 μg/mL CuS@SiO_2 NPs was observed for 14 h with the transwell migration assay (**B**). Original magnification, ×100. CuS@SiO_2 NPs suppress MMP expression. After treatment with CuS@SiO_2 NPs (0, 20, 40, or 80 μg/mL) for 24 h, HeLa cells were analyzed for MMP-2 (**C**) and MMP-9 (**D**) mRNA expression. The downregulation of MMP-2 and MMP-9 after stimulation was significant ($P<0.05$) but did not vary as a function of concentration ($P>0.05$).
Abbreviations: MMP, matrix metalloproteinase; NP, nanoparticle.

(Figures 4 and 5). However, although the direct functional proteins MMP-2 and MMP-9 decreased in tumors with CuS@SiO_2 NPs, the SRC and FAK expression increased, in contrast to the in vitro results (Figure 5). The differences between the two groups in the expression of each protein were significant ($P<0.05$), although the expression of SRC and FAK varied in vitro and in vivo. The downregulation of MMP-2 and MMP-9 provides strong evidence for the suppression of metastasis.

The transwell migration assay indicated that while the basic migration suppression was related to the treatment by CuS@SiO_2 NPs, the additional inhibitors significantly increased the suppression of HeLa cell lines (Figure 6). The differences observed in the presence and absence of inhibitors were significant ($P<0.05$), while the effects of the two types of inhibitors were not significantly different ($P>0.05$; Figure S6). Thus, there is still potential to decrease migration via the SRC/FAK signaling pathway.

The median survival of the control group (n=12) was 20 weeks, whereas the median survival of the stimulated group (n=12) was 30 weeks. There was a highly significant difference between the control group and the stimulated group (log-rank $P=0.007$; Figure 7). The median survival ratio was 1.5 (95% CI, 1.079–1.921), and the hazard ratio was 0.2544 (95% CI, 0.09397–0.6885). Hence, pre-stimulation greatly improved the survival rates of the metastasis nude mouse models.

At the end of the survival curve study, three mice from the experiment group survived, their lung samples were taken and compared with those from the control group. A significant metastasis suppression effect was observed (Figure 8A). Pre-stimulation with CuS@SiO_2 NPs seemed to decrease the metastasis of HeLa cells. The same trend was observed by histological examination (Figure 8B). Lung metastasis was widely observed in the control group (Figure 8B[a] and [b]), while metastasis was rare in the stimulated group (Figure 8B[c] and [d]).

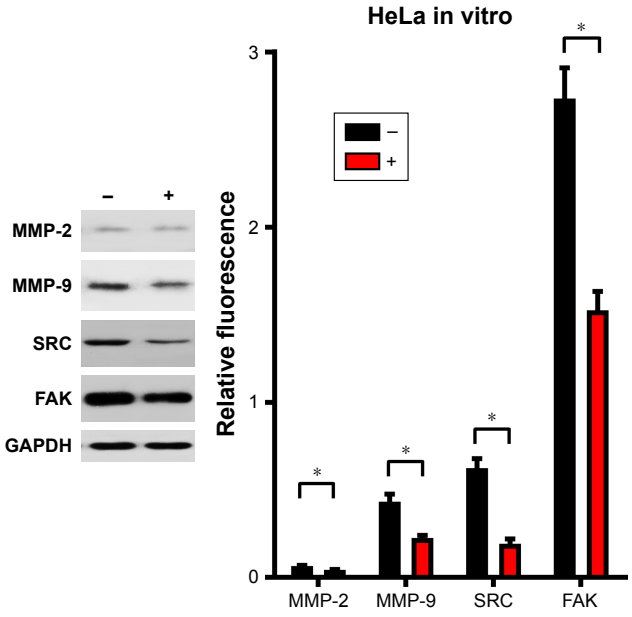

Figure 4 HeLa cells were stimulated with CuS@SiO_2 NPs (0 or 80 μg/mL) for 48 h. The expression was normalized to that of GAPDH (n=3). Statistical analysis showed significant differences after stimulation (*P<0.05). The levels of MMP-2, MMP-9, SRC, and FAK decreased. The migration of HeLa cells was suppressed by the CuS@SiO_2 NPs (80 μg/mL).
Abbreviations: FAK, focal adhesion kinase; MMP, matrix metalloproteinase; NP, nanoparticle.

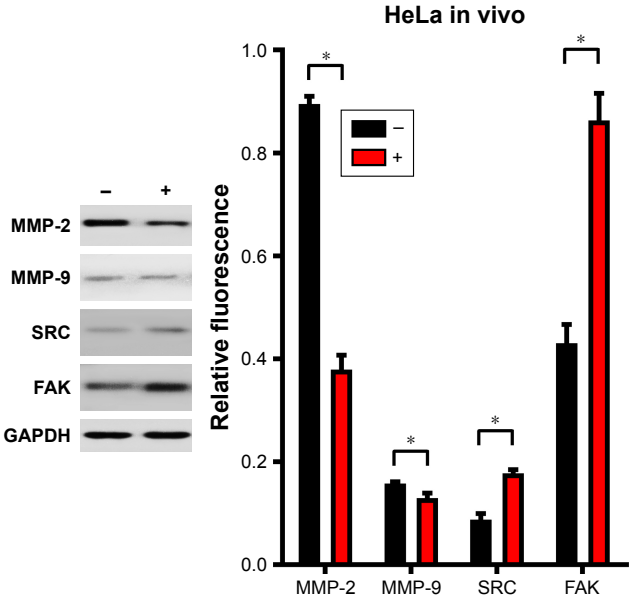

Figure 5 Subcutaneous tumors were isolated 2 weeks after subcutaneous injection of HeLa cells. The expression was normalized to that of GAPDH (n=4). Statistical analysis showed significant differences after stimulation (*P<0.05). The levels of MMP-2 and MMP-9 decreased, and the expression levels of SRC and FAK were upregulated. The migration of HeLa cells was suppressed by the CuS@SiO_2 NPs (80 μg/mL), but it may not be directly associated with SRC and FAK signaling pathway.
Abbreviations: FAK, focal adhesion kinase; MMP, matrix metalloproteinase; NP, nanoparticle.

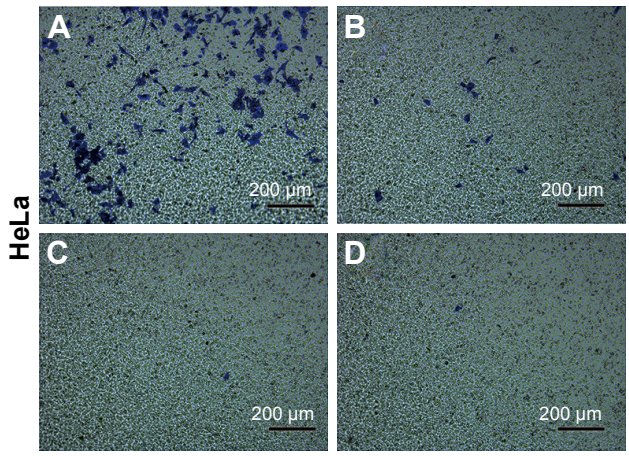

Figure 6 Representative images of the HeLa cell migration induced by CuS@SiO_2 NPs (80 μg/mL) with or without SRC/FAK inhibitors evaluated by a transwell migration assay. (**A**) Medium only group; (**B**) 80 μg/mL CuS@SiO_2 NPs; (**C**) CuS@SiO_2 NPs with 1 ng/mL FAK inhibitor; (**D**) CuS@SiO_2 NPs with 1 ng/mL SRC inhibitor. Original magnification, ×100.
Abbreviations: FAK, focal adhesion kinase; NP, nanoparticle.

Discussion

NPs alone are sufficient to modulate cellular response.[36,37] After the core index and the intervention were evaluated, a systematic experimental design was executed to ensure that the data were reliable. The absorbance and fluorescence of CuS@SiO_2 NPs were pretested to eliminate any interference in the CCK-8 tests and flow analyses. After the phenomenon discovered by a transwell migration assay, supporting evidence was collected, including the RNA expression and protein levels of the directly functional proteins MMP-2 and MMP-9. Metastasis suppression and a probable mechanism

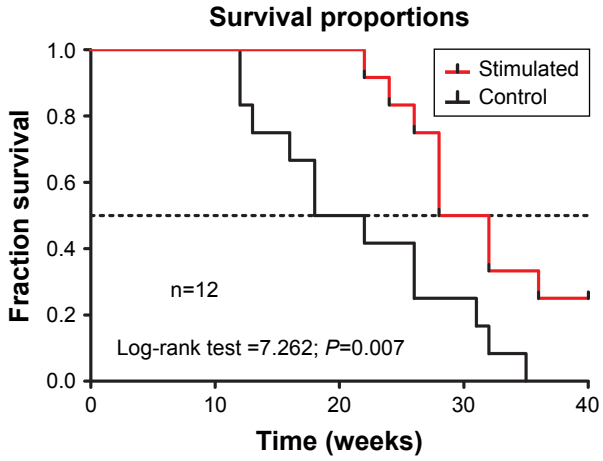

Figure 7 Kaplan–Meier survival curves for tumor metastasis in a mouse model and overall survival observed for CuS@SiO_2 NP pre-stimulation (80 μg/mL). A significant difference was detected (P<0.05).
Abbreviation: NP, nanoparticle.

were identified both in vivo and in vitro. Finally, an improved survival rate was observed in a mouse model of metastasis. Based on this evidence, we conclude that metastasis was suppressed by the CuS@SiO$_2$ NPs.

Our team has been making efforts in the practical application of photothermal technology. PTT in cancer treatment[38] is technically considered as representative of "precision medicine" with enormous potential.[39] With developments in nanotechnology, various targeting[40] and multifunctional[41] NPs that can deliver drugs and directly or indirectly kill cancer cells have been reported. However, the complex, long-term effects of NP therapy are less understood, particularly in the prevention of cancer metastasis. In oncotherapy, the effects of NP therapy clearly demand further study.[42]

The secretion of MMPs with the capacity for extracellular matrix (ECM) degradation is a feature of metastatic cancer cells.[43] MMP-2 and MMP-9 are two of the most well-characterized MMPs[44] associated with cancer invasion and metastasis due to the strong proteolysis of the ECM.[45] Consequently, MMP-2 and MMP-9 were considered a core index of migration to evaluate the function of CuS@SiO$_2$ NPs.

It is impossible to clarify the mechanism of the CuS@SiO$_2$ NPs and the factors that naturally exist in vivo. Even for growth factors with specific functions, the mechanisms still remain largely unknown. With regard to the regulation of MMP-2 and MMP-9, classical signaling pathways and explicit mechanisms have been reported. SRC and FAK are classical regulatory proteins.[44,46,47]

SRC kinase can promote the activation of the ERK, AKT, and p38 signaling pathways, the secretion of the MMPs, MMP-2 and MMP-9, and a partial epithelial–mesenchymal transition (EMT).[48] Elevated SRC kinase activity causes focal adhesion turnover.[46] In addition, SRC can phosphorylate the substrate FAK to promote cell migration.[49] The activities of SRC and FAK have been observed in many types of tumors, promoting invasion and migration,[50] and a capacity of these proteins to increase MMP-2/MMP-9 expression has also been reported.[51] Our data showed the suppression of SRC and FAK in vitro, which may explain the downregulation of MMP-2/MMP-9. However, the expression levels of SRC and FAK exert opposite effects in vivo, despite the decreased MMP-2/MMP-9.

Thus, it is likely that other potent mechanisms influence the expression of MMP-2/MMP-9. The high activity of SRC/FAK in vitro and in vivo indicates a possible signaling pathway and an unknown adjustment method. Using the transwell migration assay with SRC/FAK inhibitors, enormous suppression potential was demonstrated, supporting the different pathway hypothesis.

Conclusion

Following the mechanism discovery described earlier, survival curves ultimately verified the therapeutic effects and applicability of the CuS@SiO$_2$ NPs. The mechanisms have not been fully determined, yet the biosafety was systematically demonstrated. The reason for the long-term effects over 2 weeks is still unclear, regarding the highly improved

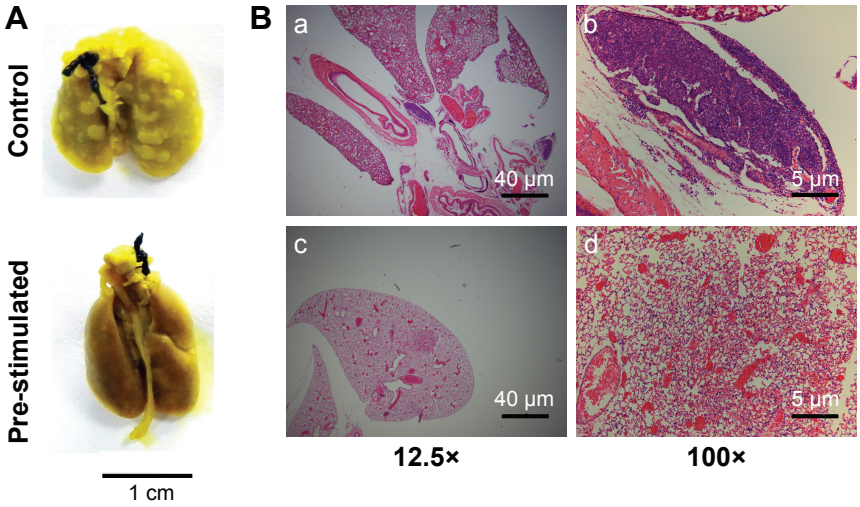

Figure 8 Histological evaluation of lung metastasis in nude mice with or without pre-stimulation by CuS@SiO$_2$ NPs. (**A**) General observation of metastasis tumors in the lungs of control mice and stimulated mice. (**B**) Hematoxylin–eosin staining of lung metastasis at low magnification (a, c) and high magnification (b, d). Nests of tumors were observed.

Abbreviation: NP, nanoparticle.

survival rates. It remains unclear whether the effects arose from toxicity leading to delayed cell death, the blocking of homing receptors, better recognition by the immune system, or the suppression of migration. However, the most important point is that the therapeutic effects were directly related to treatment by NPs; the effects in this study did not arise from loaded drugs, PTT, or other reported destruction methods but from the elements, structure, or other unknown features of the NPs. In this study, the results regarding classical signaling pathways were complicated and confusing, even contradictory. Thus, further work remains for the newly discovered phenomenon.

Acknowledgments

The authors thank Prof Hu Junqing from College of Materials Science and Engineering, Donghua University. The guidance and support was precious to the whole project. This work was supported by the Shanghai Municipal Nature Science Foundation (13ZR1433300); National Natural Science Foundation of China (Grant no 21476136); postgraduation innovation subject of Shanghai Jiao Tong University (BXJ201734); Fund for Construction of Trauma Center of Shanghai First People's Hospital (No 1304); and Songjiang District Trauma Linkage System Construction Fund (0702N14004).

Disclosure

The authors report no conflicts of interest in this work.

References

1. Caruthers SD, Wickline SA, Lanza GM. Nanotechnological applications in medicine. *Curr Opin Biotechnol*. 2007;18(1):26–30.
2. Sao R, Vaish R, Sinha N. Multifunctional drug delivery systems using inorganic nanomaterials: a review. *J Nanosci Nanotechnol*. 2015;15(3):1960–1972.
3. Lin YY, Liao JD, Ju YH, Chang CW, Shiau AL. Focused ion beam-fabricated Au micro/nanostructures used as a surface enhanced Raman scattering-active substrate for trace detection of molecules and influenza virus. *Nanotechnology*. 2011;22(18):185308.
4. Seth A, Oh DB, Lim YT. Nanomaterials for enhanced immunity as an innovative paradigm in nanomedicine. *Nanomedicine (Lond)*. 2015;10(6):959–975.
5. Lee SM, Park H, Yoo KH. Synergistic cancer therapeutic effects of locally delivered drug and heat using multifunctional nanoparticles. *Adv Mater*. 2010;22(36):4049–4053.
6. Aloi A, Vargas Jentzsch A, Vilanova N, Albertazzi L, Meijer EW, Voets IK. Imaging nanostructures by single-molecule localization microscopy in organic solvents. *J Am Chem Soc*. 2016;138(9):2953–2956.
7. Fernandez-Fernandez A, Manchanda R, McGoron AJ. Theranostic applications of nanomaterials in cancer: drug delivery, image-guided therapy, and multifunctional platforms. *Appl Biochem Biotechnol*. 2011;165(7–8):1628–1651.
8. Qu Y, Li J, Ren J, Leng J, Lin C, Shi D. Enhanced synergism of thermochemotherapy by combining highly efficient magnetic hyperthermia with magnetothermally-facilitated drug release. *Nanoscale*. 2014;6(21):12408–12413.
9. Zhou M, Chen Y, Adachi M, et al. Single agent nanoparticle for radiotherapy and radio-photothermal therapy in anaplastic thyroid cancer. *Biomaterials*. 2015;57:41–49.
10. Fan L, Zhang Y, Wang F, et al. Multifunctional all-in-one drug delivery systems for tumor targeting and sequential release of three different anti-tumor drugs. *Biomaterials*. 2016;76:399–407.
11. Liu X, Wang Q, Li C, et al. Cu(2)-xSe@mSiO(2)-PEG core-shell nanoparticles: a low-toxic and efficient difunctional nanoplatform for chemo-photothermal therapy under near infrared light radiation with a safe power density. *Nanoscale*. 2014;6(8):4361–4370.
12. El-Toni AM, Habila MA, Labis JP, et al. Design, synthesis and applications of core-shell, hollow core, and nanorattle multifunctional nanostructures. *Nanoscale*. 2016;8(5):2510–2531.
13. Enriquez-Navas PM, Wojtkowiak JW, Gatenby RA. Application of evolutionary principles to cancer therapy. *Cancer Res*. 2015;75(22):4675–4680.
14. Jiang WG, Sanders AJ, Katoh M, et al. Tissue invasion and metastasis: molecular, biological and clinical perspectives. *Semin Cancer Biol*. 2015;35(Suppl):S244–S275.
15. Valkenburg KC, Steensma MR, Williams BO, Zhong Z. Skeletal metastasis: treatments, mouse models, and the Wnt signaling. *Chin J Cancer*. 2013;32(7):380–396.
16. Zhou W, Fong MY, Min Y, et al. Cancer-secreted miR-105 destroys vascular endothelial barriers to promote metastasis. *Cancer Cell*. 2014;25(4):501–515.
17. Casey SC, Vaccari M, Al-Mulla F, et al. The effect of environmental chemicals on the tumor microenvironment. *Carcinogenesis*. 2015;36(Suppl 1):S160–S183.
18. Gao Y, Xie J, Chen H, et al. Nanotechnology-based intelligent drug design for cancer metastasis treatment. *Biotechnol Adv*. 2014;32(4):761–777.
19. Tang S, Yin Q, Su J, et al. Inhibition of metastasis and growth of breast cancer by pH-sensitive poly (beta-amino ester) nanoparticles co-delivering two siRNA and paclitaxel. *Biomaterials*. 2015;48:1–15.
20. Gupta GP, Massague J. Cancer metastasis: building a framework. *Cell*. 2006;127(4):679–695.
21. Hainaut P, Plymoth A. Targeting the hallmarks of cancer: towards a rational approach to next-generation cancer therapy. *Curr Opin Oncol*. 2013;25(1):50–51.
22. Polacheck WJ, Zervantonakis IK, Kamm RD. Tumor cell migration in complex microenvironments. *Cell Mol Life Sci*. 2013;70(8):1335–1356.
23. Yang K, Xu H, Cheng L, Sun C, Wang J, Liu Z. In vitro and in vivo near-infrared photothermal therapy of cancer using polypyrrole organic nanoparticles. *Adv Mater*. 2012;24(41):5586–5592.
24. Zha Z, Yue X, Ren Q, Dai Z. Uniform polypyrrole nanoparticles with high photothermal conversion efficiency for photothermal ablation of cancer cells. *Adv Mater*. 2013;25(5):777–782.
25. Liu X, Ren Q, Fu F, et al. CuS@mSiO2-PEG core-shell nanoparticles as a NIR light responsive drug delivery nanoplatform for efficient chemo-photothermal therapy. *Dalton Trans*. 2015;44(22):10343–10351.
26. Gilgenkrantz S. Soixante ans de cultures cellulaires HeLa. [Sixty years of HeLa cell cultures]. *Hist Sci Med*. 2014;48(1):139–144. French.
27. Chinnakkannu Vijayakumar C, Venkatakrishnan K, Tan B. Harmonizing HeLa cell cytoskeleton behavior by multi-Ti oxide phased nanostructure synthesized through ultrashort pulsed laser. *Sci Rep*. 2015;5:15294.
28. Hurst DR, Welch DR. Metastasis suppressor genes: at the interface between the environment and tumor cell growth. *Int Rev Cell Mol Biol*. 2011;286:107–180.
29. Davies KJ. The complex interaction of matrix metalloproteinases in the migration of cancer cells through breast tissue stroma. *Int J Breast Cancer*. 2014;2014:839094.
30. Cheng L, Pricolo V, Biancani P, Behar J. Overexpression of progesterone receptor B increases sensitivity of human colon muscle cells to progesterone. *Am J Physiol Gastrointest Liver Physiol*. 2008;295(3):G493–G502.
31. Chiang SP, Cabrera RM, Segall JE. Tumor cell intravasation. *Am J Physiol Cell Physiol*. 2016;311(1):C1–C14.

32. Lu JY, Chen HC, Chu RY, et al. Establishment of red fluorescent protein-tagged HeLa tumor metastasis models: determination of DsRed2 insertion effects and comparison of metastatic patterns after subcutaneous, intraperitoneal, or intravenous injection. *Clin Exp Metastasis*. 2003;20(2):121–133.
33. Adjei IM, Sharma B, Labhasetwar V. Nanoparticles: cellular uptake and cytotoxicity. *Adv Exp Med Biol*. 2014;811:73–91.
34. Kafshgari MH, Harding FJ, Voelcker NH. Insights into cellular uptake of nanoparticles. *Curr Drug Deliv*. 2015;12(1):63–77.
35. Rolny C, Mazzone M, Tugues S, et al. HRG inhibits tumor growth and metastasis by inducing macrophage polarization and vessel normalization through downregulation of PlGF. *Cancer Cell*. 2011; 19(1):31–44.
36. Setyawati MI, Kutty RV, Leong DT. DNA nanostructures carrying stoichiometrically definable antibodies. *Small*. 2016;12(40): 5601–5611.
37. Setyawati MI, Leong DT. Mesoporous silica nanoparticles as an antitumoral-angiogenesis strategy. *ACS Nano*. 2017;9(8):6690–6703.
38. Chu KF, Dupuy DE. Thermal ablation of tumours: biological mechanisms and advances in therapy. *Nat Rev Cancer*. 2014;14(3):199–208.
39. Zhu X, Feng W, Chang J, et al. Temperature-feedback upconversion nanocomposite for accurate photothermal therapy at facile temperature. *Nat Commun*. 2016;7:10437.
40. Anselmo AC, Mitragotri S. Cell-mediated delivery of nanoparticles: taking advantage of circulatory cells to target nanoparticles. *J Control Release*. 2014;190:531–541.
41. Baek S, Singh RK, Khanal D, et al. Smart multifunctional drug delivery towards anticancer therapy harmonized in mesoporous nanoparticles. *Nanoscale*. 2015;7(34):14191–14216.
42. Bohl CR, Harihar S, Denning WL, Sharma R, Welch DR. Metastasis suppressors in breast cancers: mechanistic insights and clinical potential. *J Mol Med (Berl)*. 2014;92(1):13–30.
43. Koul HK, Pal M, Koul S. Role of p38 MAP kinase signal transduction in solid tumors. *Genes Cancer*. 2013;4(9–10):342–359.
44. Huang Q, Lan F, Wang X, et al. IL-1β-induced activation of p38 promotes metastasis in gastric adenocarcinoma via upregulation of AP-1/c-fos, MMP2 and MMP9. *Mol Cancer*. 2014;13:18.
45. Watanabe A, Hoshino D, Koshikawa N, Seiki M, Suzuki T, Ichikawa K. Critical role of transient activity of MT1-MMP for ECM degradation in invadopodia. *PLoS Comput Biol*. 2013;9(5):e1003086.
46. Luo Y, Liang F, Zhang ZY. PRL1 promotes cell migration and invasion by increasing MMP2 and MMP9 expression through Src and ERK1/2 pathways. *Biochemistry*. 2009;48(8):1838–1846.
47. Xu L, Wang T, Meng W, et al. Salinomycin inhibits hepatocellular carcinoma cell invasion and migration through JNK/JunD pathway-mediated MMP9 expression. *Oncol Rep*. 2015;33(3):1057–1063.
48. Sophors P, Kim YM, Seo GY, et al. A synthetic isoflavone, DCMF, promotes human keratinocyte migration by activating Src/FAK signaling pathway. *Biochem Biophys Res Commun*. 2016;472(2):332–338.
49. Liu C, Li Y, Xing Y, et al. The interaction between cancer stem cell marker CD133 and Src protein promotes Focal Adhesion Kinase (FAK) phosphorylation and cell migration. *J Biol Chem*. 2016;291(30): 15540–15550.
50. Owens LV, Xu L, Craven RJ, et al. Overexpression of the focal adhesion kinase (p125FAK) in invasive human tumors. *Cancer Res*. 1995; 55(13):2752–2755.
51. Hsia DA, Mitra SK, Hauck CR, et al. Differential regulation of cell motility and invasion by FAK. *J Cell Biol*. 2003;160(5):753–767.

Supplementary materials

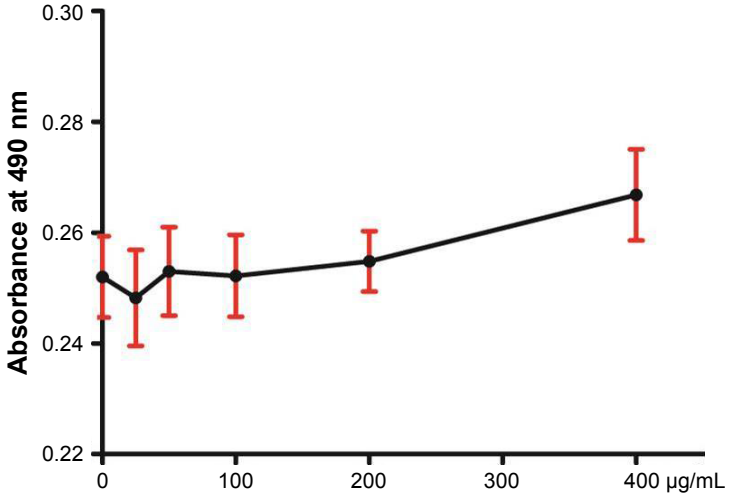

Figure S1 The absorbance of CuS@SiO_2 NPs at 490 nm was low, preventing interference with the CCK-8 test.
Abbreviations: CCK-8, Cell Counting Kit-8; NP, nanoparticle.

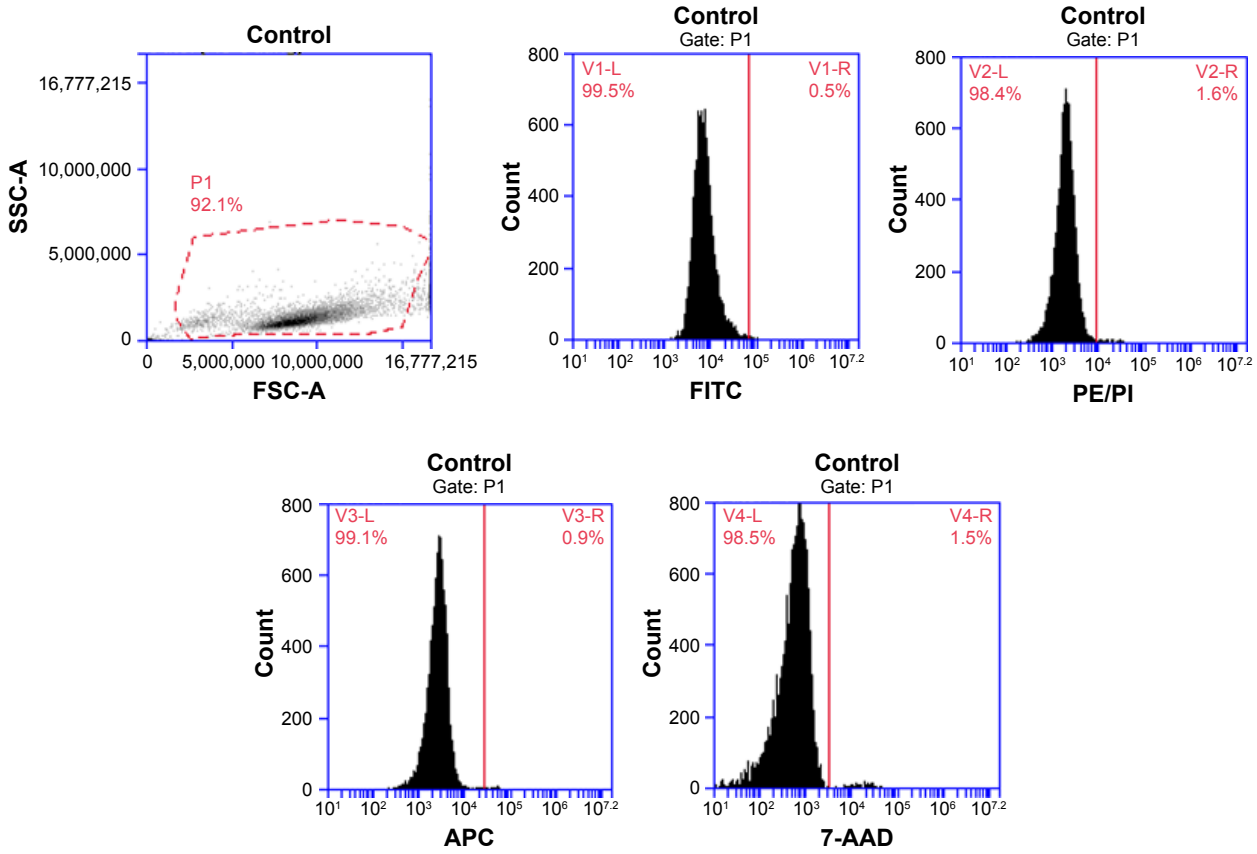

Figure S2 Flow cytometry of HeLa cells without CuS@SiO_2 NPs. The fluorescence intensities of FITC, PE/PI, 7AAD, and APC were evaluated.
Abbreviations: 7-AAD, 7-amino actinomycin D; APC, allophycocyanin; FITC, fluorescein isothiocyanate; NP, nanoparticle; PE, phycoerythrin; PI, propidium iodide.

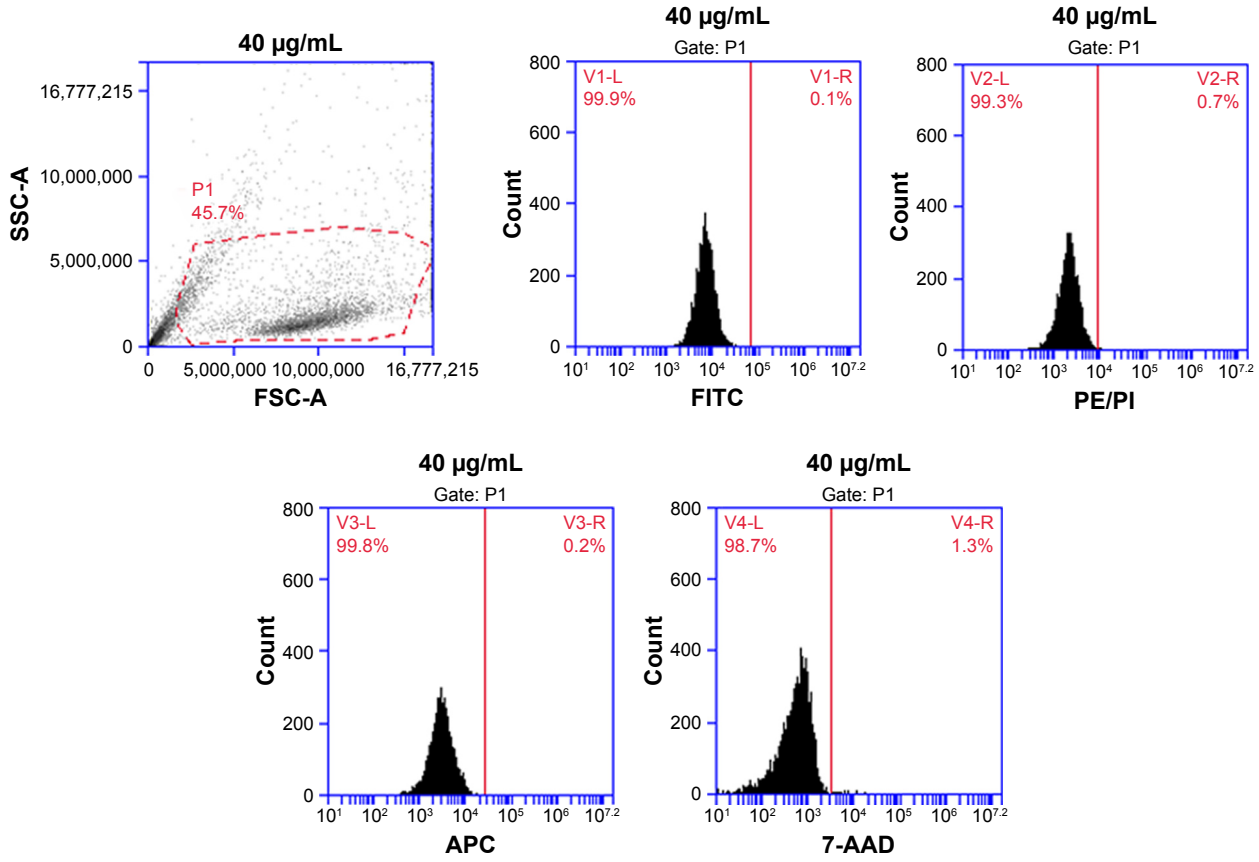

Figure S3 Flow cytometry of HeLa cells stimulated with 80 μg/mL CuS@SiO$_2$ NPs. After stimulation, the fluorescence intensities of FITC, PE/PI, 7AAD, and APC showed no significant change (Figure S1).
Abbreviations: 7-AAD, 7-amino actinomycin D; APC, allophycocyanin; FITC, fluorescein isothiocyanate; NP, nanoparticle; PE, phycoerythrin; PI, propidium iodide.

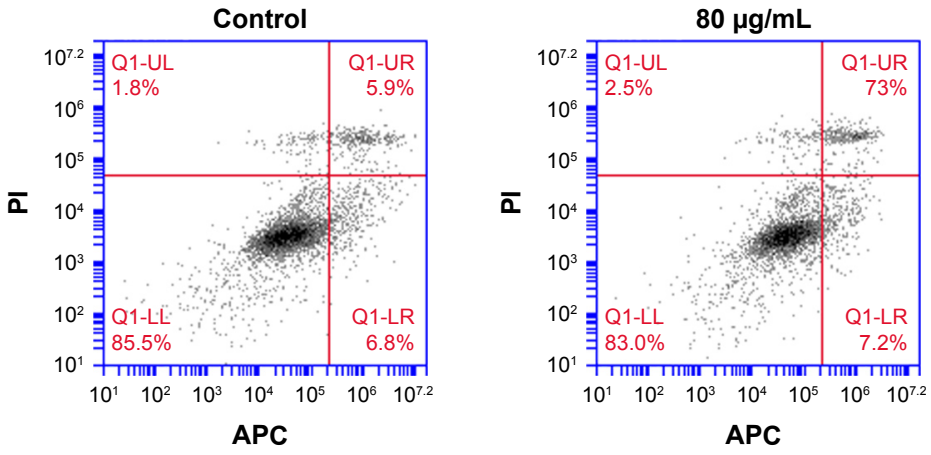

Figure S4 Flow cytometry of HeLa cells based on Annexin V–APC and PI. The apoptosis rates of HeLa cells stimulated with 80 μg/mL CuS@SiO$_2$ NPs were not significantly different from the control rates ($P>0.05$).
Abbreviations: NP, nanoparticle; PI, propidium iodide.

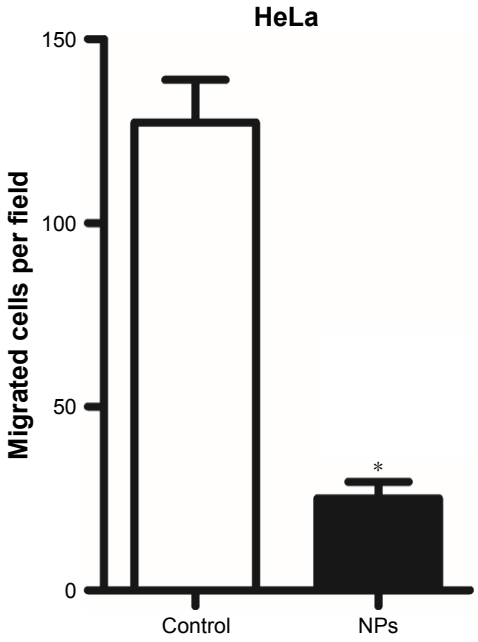

Figure S5 The number of migrated cells per field was calculated and statistically analyzed. Significant differences between the control group and the CuS@SiO_2 NP group were detected in both cancer cell lines (*$P<0.05$).
Abbreviation: NP, nanoparticle.

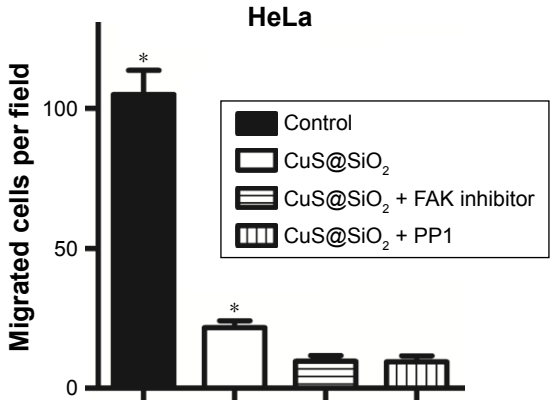

Figure S6 The number of migrated cells per field was calculated and statistically analyzed. The control group and the CuS@SiO_2 group exhibited significant differences from the other groups (*$P<0.05$), but the difference between the two inhibitor groups was not significant ($P>0.05$).
Abbreviation: FAK, focal adhesion kinase.